RAPID COMMUNICATIONS

PHYSICAL REVIEW A VOLUME 41, NUMBER 11 1 JUNE 1990

Influence of light polarization on the dynamics of optically pumped lasers

M. Arjona and R. Corbalan
Departament de Física, Universitat Autònoma de Barcelona, 08193 Bellaterra, Spain

F. Laguarta and J. Pujol
Departament d'Optica i Optometría, Universitat Politècnica de Catalunya, 08222 Terrassa, Spain

R. Vilaseca
Departament Interuniversitari d'Optica, Universitat de Valencia, 46100 Burjassot, Spain
(Received 18 December 1989)

The dynamic behavior of a coherently pumped ring laser with a homogeneously broadened four-level medium is analyzed theoretically, considering linearly polarized pump and generated laser beams. The laser is shown to be much more stable when these polarizations are parallel than when they are orthogonal. In the latter case the instability pump threshold can be as low as four times the first laser threshold, and the laser dynamics shows Lorenz-type features.

Recent experimental studies of self-pulsing in an optically pumped FIR single-mode ammonia laser showed for the first time Lorenz-like behavior in the real world.[1,2] The theoretical interpretation of these results raises conceptual difficulties, however, since the FIR laser experiments are *a priori* more complicated than the simple two-level homogeneously broadened medium interacting with a single mode of a unidirectional ring cavity, which is considered in the Lorenz-Haken model.[3,4] Recently, we have shown that a more appropriate Doppler-broadened three-level laser model can explain the appearance of Lorenz-like dynamics in an optically-pumped FIR laser.[5,6] The success of this model does not obviate, however, the study of the influence of other physical factors, previously neglected, that very likely also play an important role in the FIR laser experiments. We focus here on the influence of the polarizations of the pump and generated laser fields. In many actual FIR laser systems[1,2] the pump and laser fields, which couple to adjacent transitions in a Λ-type three-level scheme, are orthogonally polarized fields, and this aspect cannot be represented by three-nondegenerate-level laser models.[5,6] Any model that takes the vector character of the light field into account necessitates that level degeneracy related to angular momenta of the molecular states should be incorporated. Owing to the high angular momenta of the states involved in the FIR ammonia laser it seems extremely hard to describe the experimental system.[1,2] Instead, we will deal with the simplest molecular transition scheme which can give us a physical insight into the light-polarization-induced effects on the optically pumped laser dynamics.

Figure 1 illustrates the $J_a=0 \rightarrow J_b=1 \rightarrow J_c=0$ transition scheme assumed for the homogeneously broadened gain medium of an optically pumped ring laser. It is the simplest level scheme that permits the consideration of interaction with pump $\mathbf{E}_2(z,t)$ and generated $\mathbf{E}_1(z,t)$ fields composed by arbitrary superpositions of right and left circulary polarized components; moreover it is likely to display effects related to light polarization and level degeneracy in the most spectacular way. Both fields are described as uniform plane monochromatic waves propagating along the optical (z) axis of the ring resonator

$$\mathbf{E}_j(z,t)=\sum_{\mu=\pm}\mathbf{e}^{\mu}A_j^{\mu}(t)\exp\{i[k_jz-\nu_j^{\mu}t-\phi_j^{\mu}(t)]\}/2 + \text{c.c.}\ (j=1,2), \tag{1}$$

where the unit vectors $\mathbf{e}^{\pm}=\mp(\mathbf{e}_x\pm i\mathbf{e}_y)/\sqrt{2}$. The z axis is also chosen to be the quantization axis, so that only four levels are involved [the sublevel ($J_b=1,0$) does not couple to the fields], which we shall simply denote as a, $+$, $-$, and c. The A_2^{μ}, ν_2^{μ}, φ_2^{μ} characteristics of the pump beam are considered as constant in time control parameters; the unknown amplitudes A_1^{μ} and phases φ_1^{μ} of the generated beam are slowly varying functions of time. We assume that the pump beam drives the a-b transition only, and the generated field the b-c transition only.

In the rotating wave approximation the dynamics of the system molecules plus pump and generated fields in the ring cavity is governed by the following closed set of

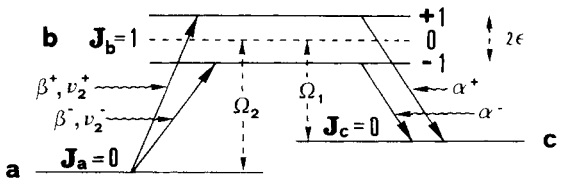

FIG. 1. Schematic representation of the level system and laser fields considered in this work. $2\beta^{\pm}$ represent the pump Rabi frequencies and $2\alpha^{\pm}$ the generated ones.

Maxwell-Schrödinger equations:

$$\dot{\rho}_{a\mu}(t) = -[\gamma_{a\mu} + i(\Delta_2^{\mu} - \mu\varepsilon)]\rho_{a\mu} - i\beta^{-\mu}\rho_{-\mu\mu} - i\beta^{\mu}(\rho_{\mu\mu} - \rho_{aa}) + i\alpha^{\mu}\rho_{ac}\exp(-i\theta\delta_{\mu-}), \tag{2a}$$

$$\dot{\rho}_{ac}(t) = -[\gamma_{ac} + i(\Delta_1^{+} - \Delta_2^{+})]\rho_{ac} - i\beta^{+}\rho_{+c} + i\alpha^{+}\rho_{a+} - i(\beta^{-}\rho_{-c} - \alpha^{-}\rho_{a-}) - \exp(i\theta), \tag{2b}$$

$$\dot{\rho}_{\mu-\mu}(t) = -[\gamma_{\mu-\mu} - i(\nu_2^{\mu} - \nu_2^{-\mu} - 2\mu\varepsilon)]\rho_{\mu-\mu} - i\beta^{\mu}\rho_{a-\mu} + i\beta^{-\mu}\rho_{\mu a} - i(\alpha^{\mu}\rho_{c-\mu} - \alpha^{-\mu}\rho_{\mu c})\exp(-i\mu\theta), \tag{2c}$$

$$\dot{\rho}_{c\mu}(t) = -[\gamma_{c\mu} + i(\Delta_1^{\mu} - \mu\varepsilon)]\rho_{c\mu} - i\alpha^{\mu}(\rho_{\mu\mu} - \rho_{cc}) + i\beta^{\mu}\rho_{ca}\exp(i\theta\delta_{\mu-1}) - i\alpha^{-\mu}\rho_{-\mu\mu}\exp(-i\mu\theta), \tag{2d}$$

$$\dot{\rho}_{\mu\mu}(t) = \gamma_{\mu}(\rho_{\mu\mu}^{0} - \rho_{\mu\mu}) + 2\alpha^{\mu}\,\mathrm{Im}(\rho_{c\mu}) + 2\beta^{\mu}\,\mathrm{Im}(\rho_{a\mu}), \tag{2e}$$

$$\dot{\rho}_{aa}(t) = \gamma_a(\rho_{aa}^{0} - \rho_{aa}) - \sum_{\mu=\pm} 2\beta^{\mu}\,\mathrm{Im}(\rho_{a\mu}), \tag{2f}$$

$$\dot{\rho}_{cc}(t) = \gamma_c(\rho_{cc}^{0} - \rho_{cc}) - \sum_{\mu=\pm} 2\alpha^{\mu}\,\mathrm{Im}(\rho_{c\mu}), \tag{2g}$$

$$\dot{\alpha}^{\mu} = -\gamma^{\mu}\alpha^{\mu}/2 + G\,\mathrm{Im}(\rho_{\mu c}), \tag{3}$$

where a dot over a quantity denotes the time derivative; ρ_{ij} $(i,j = a,+,-,c)$ are slowly varying envelopes of density matrix elements normalized to the density N^0 of molecules in the four-level system in the absence of fields. γ_i, γ_{ij}, and γ^{μ} are the population, coherence, and generated field intensity decay rates. 2ε is the Zeeman splitting between levels + and −. The field-matter coupling is characterized by four real Rabi frequencies (see Fig. 1) defined as $\beta^{\mu} = d_2 A_2^{\mu}/2\hbar$ and $\alpha^{\mu} = d_1 A_1^{\mu}/2\hbar$, with d_j $(j = 1,2)$ being molecular transition electric dipole moments. The gain parameter appearing in (3) is $G = \Omega_1 d_1^2 N^0/2\epsilon_0\hbar$. Finally, the slowly varying relative phase angle θ, and the pump and generated field detunings Δ_j^{μ} $(j = 1,2)$ are defined as

$$\theta = [(\nu_1^{+} - \nu_1^{-})t - (\nu_2^{+} - \nu_2^{-})t + (\phi_1^{+} - \phi_1^{-}) - (\phi_2^{+} - \phi_2^{-})],$$

$$\Delta_2^{\mu} = \nu_2^{\mu} - \Omega_2, \quad \Delta_1^{\mu} = \nu_1^{\mu} + \dot{\phi}_1^{\mu} - \Omega_1.$$

The actual generated laser frequencies $\nu_1^{\mu} + \dot{\phi}_1^{\mu}$ or, equivalently, the detunings Δ_1^{μ} are in general influenced by pulling and pushing effects and, therefore, are time-dependent in the unstable laser regime. The instantaneous value of Δ_1^{μ} is given by

$$\Delta_1^{\mu} = \Delta_1^{f} + G\,\mathrm{Re}(\rho_{\mu c})/\alpha^{\mu}, \tag{4}$$

where $\Delta_1^{f} = w^c - \Omega_1$ is the empty-cavity detuning. The time integration of (4) provides the time dependence of the laser phases.

Taking $\beta^{-} = \alpha^{-} = 0$ (or alternatively $\beta^{+} = \alpha^{+} = 0$) in the closed set of Eqs. (2) and (3) one obtains the three-level model equations discussed in Refs. 7 and 8, where attention was addressed to the influence of pump coherence on the laser dynamics. Here our study of the influence of the polarization of the fields on the dynamic behavior of an optically pumped laser is limited to the cases of linearly polarized pump and generated fields, with either parallel or orthogonal polarizations. For these cases one has $\epsilon = 0$, $\nu_j^{+} = \nu_j^{-}$, $\phi_j^{+} = \phi_j^{-}$ $(j = 1,2)$, $\alpha^{+} = \alpha^{-} = \alpha$, and either $\beta^{+} = \beta^{-} = \beta$ for the parallel case, or $\beta^{+} = -\beta^{-} = \beta$ for the orthogonal case. The resulting Eqs. (2) and (3) were

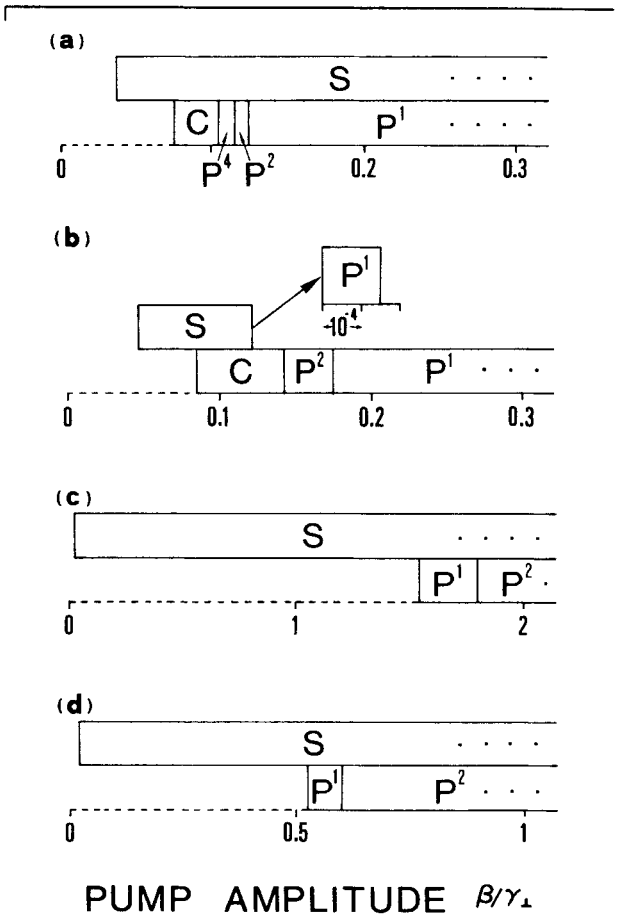

FIG. 2. Bifurcation diagrams of the optically pumped laser intensity $\alpha^2(t)$. S represents stable emission, C represents chaotic emission, and P^n represents periodic pulsing of period n. The upper strips correspond to the attractor that appears at the first laser threshold as a stable fixed point. The lower strips correspond to a second attractor whose associated dynamics develops far from steady states. For (a) and (b) the polarizations of the pump and generated fields are orthogonal; for (c) and (d) the polarizations are parallel. In (a) and (c) $\gamma_{+-} = \gamma_{\perp}$; in (b) and (d) $\gamma_{+-} = 0.5\gamma_{\perp}$. Other parameters are given in the text.

solved numerically using a seventh-eighth Runge-Kutta routine. We considered the pump field amplitude β to be the main control parameter. For other parameters, in order to permit a direct comparison with previous three-level laser results, we adopted the same values as in Ref. 7: $\gamma_{\pm c}=\gamma_\perp=6.8\times10^6$ sec^{-1}; $\gamma_\pm=\gamma_c=0.28\gamma_\perp$; $\gamma_a=\gamma_{ac}=\gamma_{\pm a}=0.95\gamma_\perp$; $\gamma^\pm=2.85\gamma_\perp$; $\Delta_2^\pm=0$; $\Delta_1^c=0$; $G=7285\gamma_\perp^2$; and

$$\rho_{aa}^0:\rho_{++}^0:\rho_{--}^0:\rho_{cc}^0=0.9594:0.0113:0.0113:0.0180\,.$$

Different values have been adopted for the newly introduced relaxation rate γ_{+-} of the coherence between the upper levels. As a first step, restricting ourselves to moderate pump powers ($\beta<0.3\gamma_\perp$), we determined the range of γ_{+-} values [$\geq 0.28\gamma_\perp=\frac{1}{2}(\gamma_++\gamma_-)$] for which the coherently pumped laser showed instabilities. With orthogonal polarizations this occurred for $\gamma_{+-}\geq 0.32\gamma_\perp$, while in the parallel case instabilities were present even at the lowest γ_{+-} value. In the following we show results for two different values: $\gamma_{+-}=0.5\gamma_\perp$ and $\gamma_{+-}=\gamma_\perp$.

As in Ref. 7, we have found two coexisting attractors in the phase space of our system, whose bifurcation diagrams for increasing pump field strength β are shown in Figs. 2(a) and 2(b) for the case of orthogonal polarizations, with $\gamma_{+-}=\gamma_\perp$ and $\gamma_{+-}=0.5\gamma_\perp$, respectively. The bifurcation diagrams for the parallel case are represented in Figs. 2(c) and 2(d) for $\gamma_{+-}=\gamma_\perp$ and $\gamma_{+-}=0.5\gamma_\perp$, respectively. The different dynamic regimes associated with these attractors are indicated as they appear on the generated intensity $\alpha^2(t)$. The first attractor [upper strip in Figs. 2(a)–2(d)] appears at the first laser threshold as a fixed point associated with the steady lasing state and, if β is increased adiabatically, remains so until it eventually [see Fig. 2(b)] undergoes a supercritical Hopf bifurcation to a small-amplitude limit cycle which turns out to be stable only in a very small domain of β values.

Starting with the laser in the $\alpha=0$ state and switching abruptly the pump field, the laser reaches a second attractor [lower strip in Figs. 2(a)–2(d)]. Note that this attractor coexists with the stable fixed point attractor [see Figs. 2(a), 2(c), and 2(d)] and appears long before the Hopf bifurcation of Fig. 2(b). All this is possible because the dynamics in the second attractor develops far away from steady states [see Fig. 3(a)]. Therefore the onset of this

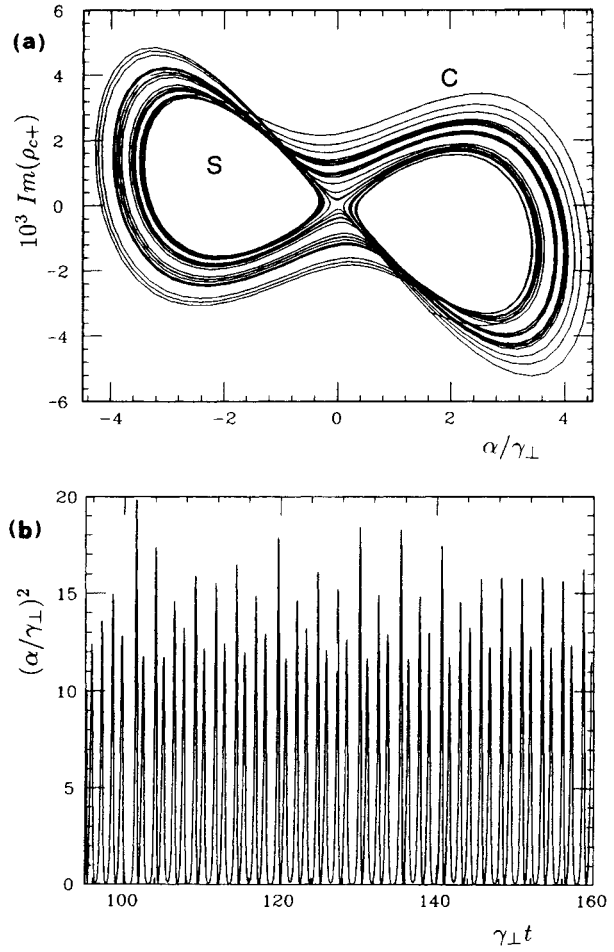

FIG. 3. (a) Two-dimensional (α,Imρ_{c+}) picture of the two attractors of Fig. 2(a) for $\beta=0.09\gamma_\perp$; (b) corresponding chaotic pulsing.

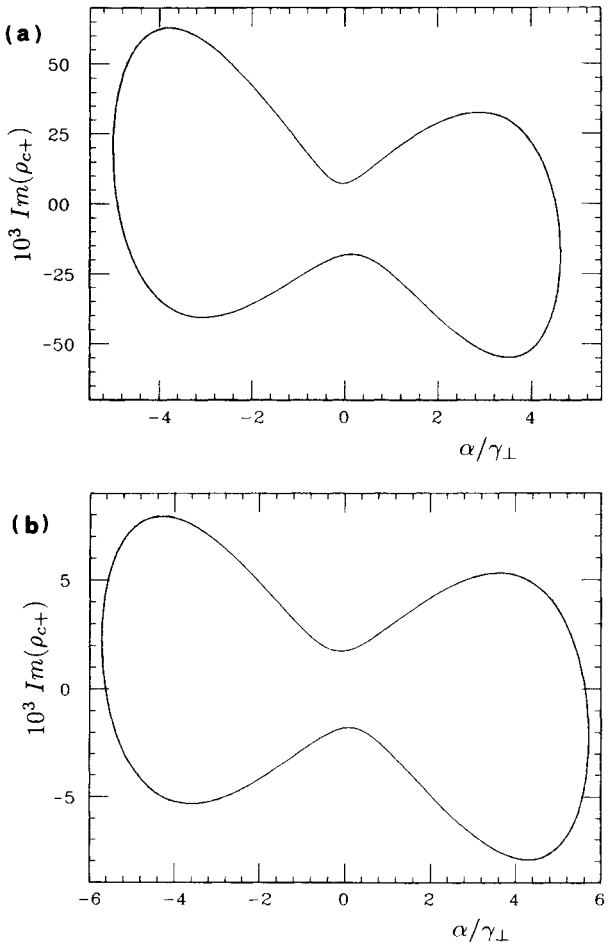

FIG. 4. Two-dimensional (α,Imρ_{c+}) projections of the second attractor in Fig. 2(a) for (a) $\beta=0.12\gamma_\perp$, (b) $0.15\gamma_\perp$.

attractor determines the laser instability threshold. A comparison of Figs. 2(a) and 2(b) with Figs. 2(c) and 2(d) shows that the optically pumped laser is much more stable operating with parallel polarizations than with the orthogonal configuration. In fact, while the instability pump threshold is $\beta/\gamma_\perp = 0.0743$ for chaotic emission (C) in Fig. 2(a), it is increased to $\beta/\gamma_\perp = 1.54$ for regular period-one pulsing (P^1) in Fig. 2(c). Note also that while the ratio $r = \beta_{\text{uns}}^2/\beta_{\text{cw}}^2$ between threshold pump intensities for unstable and cw laser emission in as low as $r = 3.88$ and 6.38 for Figs. 2(a) and 2(b), respectively, it is as high as $r = 3723$ and 498 for Figs. 2(c) and 2(d), respectively. Probably this influence of the polarization of the fields is at the origin of the different behaviors observed[9] for the 81-μm $^{14}NH_3$ transition and the 374-μm $^{15}NH_3$ transition. Of course, this conjecture needs further study in view of the different relaxation rates for these two systems. Note also in Fig. 2 that while the instability pump threshold for the orthogonal case decreases with increasing the γ_{+-} value, it increases in the parallel case. (The lowest values in the latter case are $\beta/\gamma_\perp = 0.2067$, $r = 97$, which occur for the case $\gamma_{+-} = 0.28\gamma_\perp$, not shown in Fig. 2). Therefore, phase-interrupting collisions (which increase the γ_{+-} rate over its lowest value related to the decay of molecular states) can influence the laser dynamics in dramatically different ways depending on the configuration of the light polarizations involved.

A comparison between the results in Figs. 2 and 3 and those of Ref. 7 shows large discrepancies concerning (i) the ratio r between pump intensities for unstable and cw laser emission, which was $r = 75$ in Ref. 7; (ii) the shape of the second attractor, which was asymmetric in Ref. 7, whereas in the orthogonal case is now of the symmetric-type[2] or Lorenz-type [see Fig. 3(a)], with trajectories revolving about two stable foci (the point S and its symmetric with respect to the origin); and (iii) the bifurcation diagrams, which for the orthogonal configuration show a remarkable qualitative agreement with Lorenz's model predictions.[4(a)] Note in particular that, as in the Lorenz model, the inverse period-doubling bifurcations $P^2 \rightarrow P^1$ out of chaos of Figs. 2(a) and 2(b) are not true local bifurcations but occurs through a process of progressive symmetrization of the attractor as can be appreciated in Fig. 4.

Work supported by the Dirección General de Investigación Científica y Técnica (Spain), Project No. PB86-0650-C03-00.

[1] C. O. Weiss and J. Brock, Phys. Rev. Lett. **57**, 2804 (1986).

[2] C. O. Weiss, N. B. Abraham, and U. Hübner, Phys. Rev. Lett. **61**, 1587 (1988).

[3] E. N. Lorenz, J. Atmos. Sci. **20**, 130 (1963); H. Haken, Phys. Lett. **53A**, 77 (1975).

[4] (a) H. Zeghlache and P. Mandel, J. Opt. Soc. Am. B **2**, 18 (1985); (b) H. Zeghlache, P. Mandel, N. B. Abraham, and C. O. Weiss, Phys. Rev. A **38**, 3128 (1988).

[5] R. Corbalan, F. Laguarta, J. Pujol, and R. Vilaseca, Opt. Commun. **71**, 290 (1989).

[6] E. Roldan, G. J. de Valcarcel, R. Vilaseca, F. Silva, J. Pujol, R. Corbalan, and F. Laguarta, Opt. Commun. **73**, 506 (1989).

[7] J. Pujol, F. Laguarta, R. Vilaseca, and R. Corbalan, J. Opt. Soc. Am. B **5**, 1004 (1988).

[8] J. V. Moloney, W. Forysiak, J. S. Uppal, and R. G. Harrison, Phys. Rev. A **39**, 1277 (1989), and references therein.

[9] M. P. Sassi, M. Barbeau, and C. O. Weiss, Appl. Phys. B **43**, 179 (1987).